

Article

# A FEM-Green Approach for Magnetic Field Problems with Open Boundaries

Jacques Lobry

Department of General Physics, Faculty of Engineering, University of Mons, B-7000 Mons, Belgium; jacques.lobry@umons.ac.be; Tel.: +32-65374046

**Abstract:** A new finite element method/boundary element method (FEM/BEM) scheme is proposed for the solution of the 2D magnetic static and quasi-static problems with unbounded domains. The novelty is an original approach in the treatment of the outer region. The related domain integral is eliminated at the discrete level by using the finite element approximation of the fundamental solutions (Green's functions) at every node of the related mesh. This "FEM-Green" approach replaces the standard boundary element method. It is simpler to implement because no integration on the boundary of the domain is required. Then, the method leads to a substantially reduced computational burden. Moreover, the coupling with finite elements is more natural since it is based on the same Galerkin approximation. Some examples with open boundary and nonlinear materials are presented and compared with the standard finite element method.

**Keywords:** magnetostatics; eddy-currents; Green functions; boundary element-finite element coupling; Poisson problem; nonlinear material



**Citation:** Lobry, J. A FEM-Green Approach for Magnetic Field Problems with Open Boundaries. *Mathematics* **2021**, *9*, 1662. <https://doi.org/10.3390/math9141662>

Academic Editor: Alberto Ferrero

Received: 8 June 2021

Accepted: 13 July 2021

Published: 15 July 2021

**Publisher's Note:** MDPI stays neutral with regard to jurisdictional claims in published maps and institutional affiliations.



**Copyright:** © 2021 by the author. Licensee MDPI, Basel, Switzerland. This article is an open access article distributed under the terms and conditions of the Creative Commons Attribution (CC BY) license (<https://creativecommons.org/licenses/by/4.0/>).

## 1. Introduction

A large number of electromagnetic problems involve finding fields in the vicinity of devices embedded in an infinite domain. However, classical volume discretization methods, such as the finite element method, are inherently inapplicable. Various strategies have been developed over the years, such as simple truncation of outer boundaries, ballooning, conformal mappings, infinite elements, hybrid finite element method (FEM)-boundary element method (BEM) schemes, and others. An excellent review is given in [1]. More specifically, FEM/BEM methods exploit the flexibility of the FEM for the treatment of nonhomogeneous and nonlinear materials, and the ability of the BEM to consider open regions [2]. The FEM is generally based on the Galerkin approximation of a weak or variational formulation, while the standard BEM is normally deduced from the Green's second identity for reducing domain integrals into boundary ones [3].

Instead of this classical BEM approach, in this paper, we propose an alternative so-called FEM-Green formulation as first described by the author in [4,5]. It is obtained by using the FEM approximation of fundamental solutions (Green's functions) [6,7] and consists of a discrete equivalent of the second Green's identity. More precisely, the domain integral of the open domain is naturally canceled by a combination of the Galerkin formulation of the boundary value problem under study, and the one associated with the fundamental solution for the Dirac delta loading every node of a finite element mesh of this region. The layer of finite elements that are adjacent to the boundary of the FEM region is only required with our method. Any extended mesh in some parts of the outer domain is used for the computation of fields at a postprocessing step.

The implementation of this new scheme is simpler as no boundary integration, either analytical or numerical (Gaussian quadrature), on the FEM/BEM interface is required and the coupling with the standard FEM used in the inner part of the problem appears to be extremely natural. In the two previous papers of the author, the mathematical developments

were neither presented with a source term nor in the context of magnetic field problems. Indeed, those problems have their own specificities such as a large difference of permeability between air and ferromagnetic materials. Moreover, time-harmonic eddy-current problems are described here by a complex-valued equation, which was not considered before. Thus, it is worth exploring the applicability of our method to such problems. It is the objective of the present paper. Therefore, the method is applied to 2D magnetostatic and eddy-current open boundary problems and some practical examples with open boundary and nonlinear domains are presented in the last section in order to assess the performance of our method.

## 2. Mathematical Model Description

Various FEM/BEM hybrid methods are used for the computation of open boundary problems where the classical BEM formulation is used for the treatment of the open region. Green's second identity is normally employed to derive a boundary-only formulation, avoiding the discretization of the domain. The principle of the proposed method is different and is based upon a special FEM treatment using the fundamental solution (Green's function) of the boundary value problem. This allows for a direct elimination of the domain integral at the discrete level through a Galerkin approach.

The method is presented in the context of the modified Helmholtz problem describing time-harmonic two-dimensional quasi-static problems by using magnetic vector potential (MVP)  $A$  and the magnetostatics situation as a particular case. Magnetic vector potential possesses only a longitudinally directed component denoted as  $A$  (also commonly called magnetic vector potential), so that the magnetostatic vector Poisson equation degenerates to its scalar counterpart that is stated here below. Since the 2D aspect is not mandatory for the method, it could be extended to 3D problems. This speculation is valid for scalar potential problems, e.g., in electrostatics using the scalar electric potential, as it is mostly the case, or in 3D magnetostatics using a magnetic scalar potential [8]. However, it should be fully analyzed for magnetic field problems using full MVP. Figure 1 depicts the general 2D configuration where  $\Omega_1$  is the open region (air), including the source region  $\Omega_s$  with current density  $J_s$ , and  $\Omega_2$  is the inner region that can be nonhomogeneous and/or nonlinear and/or with eddy-currents, depending on whether a magnetostatic or an eddy-current analysis is considered.

Permeability  $\mu$  and conductivity  $\sigma$  are assumed as essential material properties and we consider no Dirichlet or Neumann boundary condition for the sake of simplicity in the mathematical description of the method. The governing equations are:

$$\nabla^2 A = -\mu_0 J_s \quad \text{in } \Omega_1, \quad (1a)$$

and

$$\nabla^2 A - j\omega\sigma\mu A = 0 \quad \text{in } \Omega_2, \quad (1b)$$

while the following continuity conditions hold on the interface  $\Gamma_{int}$ :

$$A_1 = A_2 \quad \text{and} \quad \frac{1}{\mu_0} \frac{\partial A}{\partial n} \Big|_1 = \frac{1}{\mu} \frac{\partial A}{\partial n} \Big|_2. \quad (2)$$

Potential  $A$  and current density  $J_s$  are represented in phasor form with angular frequency  $\omega$  in case of a time-harmonic analysis.

### 2.1. The FEM-Green Formulation

The FEM-Green formulation is applied to the open region  $\Omega_1$  and is derived from a finite element mesh. It is first assumed that domain  $\Omega_1$  is bounded by the interface  $\Gamma_{int}$  and a remote boundary  $\Gamma_\infty$  where the homogeneous Dirichlet boundary condition ( $A = 0$ ) is considered (Figure 1). The mathematical treatment will show that the domain integral vanishes so that only a layer of finite elements along the interface  $\Gamma_{int}$  is required and there will be no problem when outer boundary  $\hat{\Gamma}_\infty$  extends to infinity.

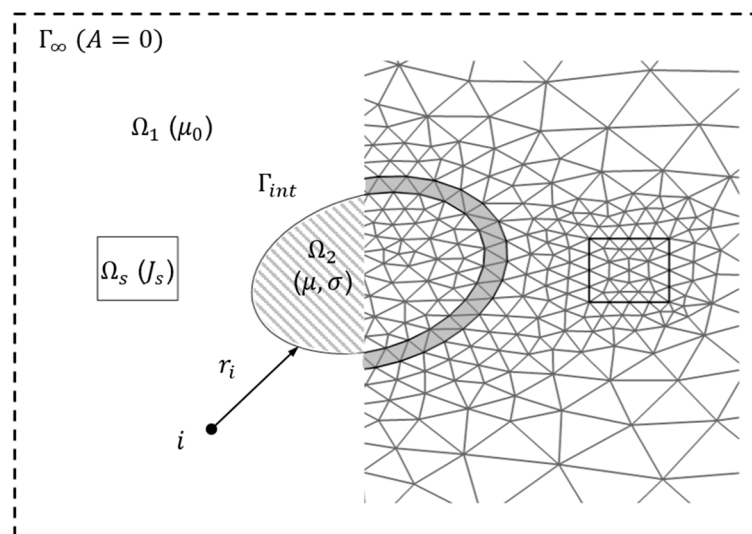


Figure 1. General configuration for the 2D modified Helmholtz problem and the FEM/FEM-Green treatment.

Mathematical treatment used here is classical and can be found in many standard books such as [9]. Consider the well-known Galerkin problem related to Poisson’s Equation (1a):

$$\int_{\hat{\Omega}_1} \nabla \hat{A} \cdot \nabla N_j \, d\Omega = \int_{\hat{\Omega}_s} \mu_0 J_s N_j \, d\Omega \quad \forall j \in \hat{\Omega}_1 \setminus \hat{\Gamma}_\infty, \quad \hat{A} = 0 \text{ on } \hat{\Gamma}_\infty, \tag{3}$$

where the  $N_j$ ’s are the classical interpolation functions defined on finite element meshes  $\hat{\Omega}_1$  and  $\hat{\Omega}_s$  of the domains  $\Omega_1$  and  $\Omega_s$ , respectively (Figure 1). We will assume first-order triangular elements for the sake of clarity in the presentation of the method. The approximate solution  $\hat{A}$  is given by:

$$\hat{A} = \sum_{k \in \hat{\Omega}_1} N_k \hat{A}_k. \tag{4}$$

The combination of Equations (3) and (4) leads to a sparse system of linear equations, of which the matrix entries are of the form:

$$s_{jk} = \int_{\hat{\Omega}_1} \nabla N_j \cdot \nabla N_k \, d\Omega. \tag{5}$$

Let us denote

$$\Phi_{\hat{A}, \Sigma_j} = \int_{\hat{\Omega}_1} \nabla \hat{A} \cdot \nabla N_j \, d\Omega = \sum_{k \in \hat{\Omega}_1} s_{jk} \hat{A}_k \quad \forall j \in \hat{\Omega}_1. \tag{6}$$

It is demonstrated in [10] that this term corresponds physically to the inward flux of  $\nabla \hat{A}$  across the “box”  $\Sigma_j$  associated with node  $j$  in the dual mesh obtained from the barycentric subdivision of the primal 2D mesh. In particular, at a node  $j$  belonging to the discretization of the interface  $\Gamma_{int}$  between  $\Omega_1$  and  $\Omega_2$ , the quantity  $\Phi_{\hat{A}, \Sigma_j}$  is interpreted as the flux through the “cap”  $\Sigma_j$ , as shown in Figure 2.

However, this interpretation is only valid for first-order elements, and it is not the case of higher-order elements where it is a mere mathematical equivalent variable. Yet, this variable obeys a continuity condition across the interface, as will be shown in Section 2.2. Parameters  $\Phi_{\hat{A}, \Sigma_j}$  are used here instead of the approximation of the normal derivative that is normally present in the classical boundary element method [3].

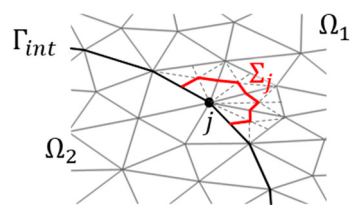


Figure 2. Typical finite element triangular mesh and barycentric “cap”  $\Sigma_j$  for an interface node  $j$ .

As in the standard BEM, the 2D fundamental solution  $\mathcal{G}_i = -1/2\pi \ln r_i$  of Laplace’s equation is exploited in order to eliminate the domain integral. Let us recall that it is obtained from the equation

$$\nabla^2 \mathcal{G}_i = -\delta_i \text{ in } \Omega_1, \text{ with } \mathcal{G}_i = -\frac{1}{2\pi} \ln r_i \text{ on } \partial\Omega_1, \tag{7}$$

where  $\delta_i$  is the Dirac delta function at any point  $i$  (Figure 1).

A FEM solution exists [6,7], and is readily derived from the Galerkin problem associated with the formulation (7):

$$\int_{\hat{\Omega}_1} \nabla \hat{\mathcal{G}}_i \cdot \nabla N_j \, d\Omega = \int_{\hat{\Omega}_1} \delta_i N_j \, d\Omega \quad \forall j \in \hat{\Omega}_1 \setminus \partial\hat{\Omega}_1, \hat{\mathcal{G}}_i = \mathcal{G}_i \text{ on } \partial\hat{\Omega}_1, \tag{8}$$

where the FEM solution  $\hat{\mathcal{G}}_i$  is interpolated as

$$\hat{\mathcal{G}}_i = \sum_{j \in \hat{\Omega}_1} N_j \hat{\mathcal{G}}_{i,j}. \tag{9}$$

An illustrative example of the FEM solution  $\hat{\mathcal{G}}_i$  of a Green’s function  $\mathcal{G}_i$  on an arbitrary domain  $\Omega$  is given in Figure 3.

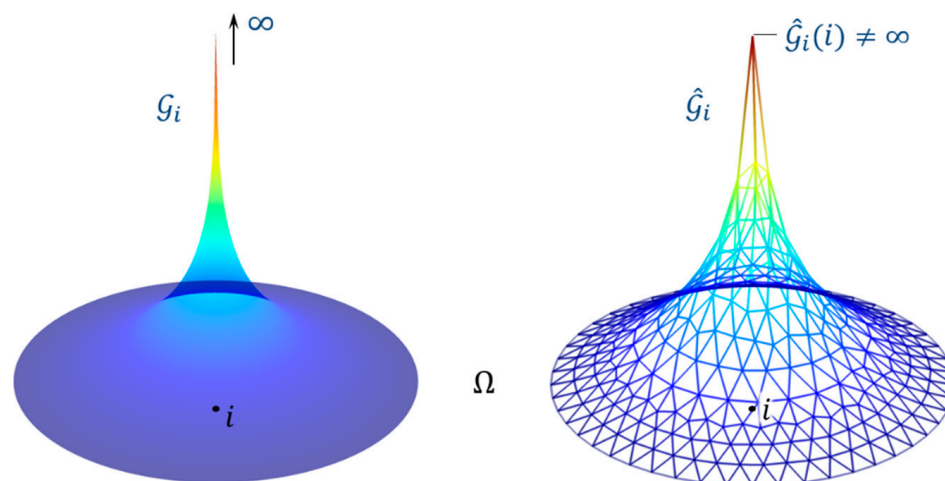


Figure 3. Example of the FEM discretization of a Green’s function on a domain  $\Omega$ .

In the same way as for  $\hat{A}$  given by (6), we can write the nodal approximation:

$$\Phi_{\hat{\mathcal{G}}_i, \Sigma_j} = \int_{\hat{\Omega}_1} \nabla \hat{\mathcal{G}}_i \cdot \nabla N_j \, d\Omega = \sum_{k \in \hat{\Omega}_1} s_{jk} \hat{\mathcal{G}}_{i,k} \quad \forall j \in \hat{\Omega}_1. \tag{10}$$

Note that  $\Phi_{\hat{\mathcal{G}}_i, \Sigma_i} = 1$ , as a consequence of Gauss’s law for any internal node  $i$  of the mesh  $\hat{\Omega}_1$ . If we combine Equations (3)–(6) and (9), a little algebra suffices to show that:

$$\int_{\hat{\Omega}_1} \nabla \hat{A} \cdot \nabla \hat{\mathcal{G}}_i \, d\Omega = \sum_{j \in \hat{\Omega}_1} \left( \sum_{k \in \hat{\Omega}_1} s_{jk} \hat{A}_k \right) \hat{\mathcal{G}}_{i,j} = \sum_{j \in \hat{\Omega}_1 \setminus \partial \hat{\Omega}_1} \int_{\hat{\Omega}_s} \mu_0 J_s N_j \, d\Omega \hat{\mathcal{G}}_{i,j} + \sum_{j \in \partial \hat{\Omega}_1} \Phi_{\hat{A}, \Sigma_j} \hat{\mathcal{G}}_{i,j} \tag{11}$$

By performing integration of the source term, (11) becomes:

$$\int_{\hat{\Omega}_1} \nabla \hat{A} \cdot \nabla \hat{\mathcal{G}}_i \, d\Omega = \sum_{j \in \hat{\Omega}_1} \left( \sum_{k \in \hat{\Omega}_1} s_{jk} \hat{A}_k \right) \hat{\mathcal{G}}_{i,j} = \mu_0 J_s \sum_{j \in \hat{\Omega}_s} \sum_{\Delta_j \in \mathcal{T}_{s,j}} \frac{|\Delta_j|}{3} \hat{\mathcal{G}}_{i,j} + \sum_{j \in \partial \hat{\Omega}_1} \Phi_{\hat{A}, \Sigma_j} \hat{\mathcal{G}}_{i,j}, \tag{12}$$

where  $\mathcal{T}_{s,j}$  is the set of triangles  $\Delta_j$  of the source region  $\hat{\Omega}_s$  sharing the node  $j$  and  $|\Delta_j|$  denotes the area of the triangle.

Conversely, using (4), adapted to  $\hat{\mathcal{G}}_i$  and Equation (10) instead of (6), we can easily write:

$$\int_{\hat{\Omega}_1} \nabla \hat{\mathcal{G}}_i \cdot \nabla \hat{A} \, d\Omega = \sum_{j \in \hat{\Omega}_1} \left( \sum_{k \in \hat{\Omega}_1} s_{jk} \hat{\mathcal{G}}_{i,k} \right) \hat{A}_j = \hat{A}_i + \sum_{j \in \partial \hat{\Omega}_1} \Phi_{\hat{\mathcal{G}}_i, \Sigma_j} \hat{A}_j. \tag{13}$$

Now, by equating (12) to (13), we can write the following expression:

$$\hat{A}_i + \sum_{j \in \hat{\Gamma}_{int}} \Phi_{\hat{\mathcal{G}}_i, \Sigma_j} \hat{A}_j = \sum_{j \in \hat{\Gamma}_{int}} \hat{\mathcal{G}}_{i,j} \Phi_{\hat{A}, \Sigma_j} + \mu_0 J_s \sum_{j \in \hat{\Omega}_s} \sum_{\Delta_j \in \mathcal{T}_{s,j}} \frac{|\Delta_j|}{3} \hat{\mathcal{G}}_{i,j}, \tag{14}$$

where the domain contribution is eliminated as announced previously, and  $\partial \hat{\Omega}_1$  has been replaced by  $\hat{\Gamma}_{int}$  since it is now licit to extend  $\hat{\Gamma}_\infty$  the outer boundary at infinity. Equation (14) can be regarded as a discrete equivalent of Green’s second identity that has been derived directly from the Galerkin approach.

Henceforth, it is necessary to write (14) for all the nodes  $i$  belonging to the boundary  $\hat{\Gamma}_{int}$ , in order to derive a consistent linear system of equations. However, due to the singularity of the  $\mathcal{G}_i$  function, the boundary condition of the problem (7) must be changed as:

$$\mathcal{G}_i = -\frac{1}{2\pi} \ln r_i \text{ on } \hat{\Gamma}_{int} \setminus \{i\} \text{ and } \frac{\partial \mathcal{G}_i}{\partial n} = 0 \text{ at } \{i\}, \tag{15}$$

so that the Galerkin formulation (8) is replaced by:

$$\int_{\hat{\Omega}_1} \nabla \hat{\mathcal{G}}_i \cdot \nabla N_j \, d\Omega = \delta_{ij} c_i \quad \forall j \in (\hat{\Omega}_1 \setminus \hat{\Gamma}_{int}) \cup \{i\}, \hat{\mathcal{G}}_i = \mathcal{G}_i \text{ on } \hat{\Gamma}_{int} \setminus \{i\}, \tag{16}$$

where  $\delta_{ij}$  is the common Kronecker symbol and  $c_i$  is the classical geometric factor of standard BEM, i.e., it is equal to the ratio  $\theta_i/2\pi$ , where  $\theta_i$  is the internal (with respect to the FEM region  $\Omega_2$ ) angle at node  $i$  [3]. It is easy to show that, in the FEM-Green context:

$$c_i = \Phi_{\hat{\mathcal{G}}_i, \Sigma_i} \quad \text{and} \quad c_i + \sum_{j \in \hat{\Gamma}_{int} \setminus \{i\}} \Phi_{\hat{\mathcal{G}}_i, \Sigma_j} = 1, \tag{17}$$

that can again be interpreted as Gauss’s law at the discrete level. Finally, the FEM-Green scheme leads to the system of the  $n$  simultaneous equations:

$$\sum_{j \in \hat{\Gamma}_{int}} \Phi_{\hat{\mathcal{G}}_i, \Sigma_j} \hat{A}_j - \sum_{j \in \hat{\Gamma}_{int}} \hat{\mathcal{G}}_{i,j} \Phi_{\hat{A}, \Sigma_j} = \mu_0 J_s \sum_{j \in \hat{\Omega}_s} \sum_{\Delta_j \in \mathcal{T}_{s,j}} \frac{|\Delta_j|}{3} \hat{\mathcal{G}}_{i,j} \quad \forall i \in \partial \hat{\Omega}_1, \tag{18}$$

where potential  $\hat{A}_j$  and flux  $\Phi_{\hat{A}, \Sigma_j}$  values are the unknown parameters along the interface  $\hat{\Gamma}_{int}$ .

At this point, the solution of (18) requires the computation of the FEM approximations  $\hat{\mathcal{G}}_i$  that is highly time consuming and does not make sense since  $\hat{\Omega}_1$  is unbounded in the context of open boundary problems. Then, coefficients  $\Phi_{\hat{\mathcal{G}}_i, \Sigma_j}$  and  $\hat{\mathcal{G}}_i$  are modified by using the *exact* fundamental solutions  $\mathcal{G}_i$  instead of  $\hat{\mathcal{G}}_i$ . More precisely the following *interpolant* should be considered:

$$\mathcal{G}_{i,l} = \sum_{j \in \Omega_1} N_j \mathcal{G}_i(j) = - \sum_{j \in \Omega_1} N_j \frac{1}{2\pi} \ln r_{ij}, \tag{19}$$

where  $r_{ij}$  is the distance between nodes  $i$  and  $j$ . However, the infinite value  $\mathcal{G}_i(i)$  must be replaced by a value  $\mathcal{G}_{i,i}^*$  that can be derived from the discrete Gauss's law (17), i.e.,

$$\hat{c}_i = \sum_{k \neq i} s_{ik} \mathcal{G}_i(k) + s_{ii} \mathcal{G}_{i,i}^* \tag{20a}$$

and:

$$\hat{c}_i + \sum_{j \in \hat{\Gamma}_{int} \setminus \{i\}} \left( \sum_{k \neq i} s_{jk} \mathcal{G}_i(k) + s_{ji} \mathcal{G}_{i,i}^* \right) = 1, \tag{20b}$$

Parameter  $\hat{c}_i$  can be considered as an estimate of the geometric factor  $c_i$  described above. By eliminating this parameter between Equations (20a) and (20b), after some algebra that we skip for the sake of conciseness, we obtain the expression of  $\mathcal{G}_{i,i}^*$ :

$$\mathcal{G}_{i,i}^* = \frac{1 - \sum_{j \in \hat{\Gamma}_{int}} \sum_{k \neq i} s_{jk} \mathcal{G}_i(k)}{\sum_{j \in \hat{\Gamma}_{int}} s_{ji}}. \tag{21}$$

As outlined above, meshing the whole domain  $\hat{\Omega}_1$  is not a necessity since the internal nodes are not involved in (18). In fact, that would not make sense since this outer region is unbounded. A *single layer* of finite elements along the boundary  $\partial\Omega_1$  (in gray in Figure 1) is sufficient. Any internal mesh of  $\Omega_1$  is used for field calculation at a postprocessing step.

By comparing with the implementation of the boundary element method, no cumbersome analytical or numerical (Gaussian quadrature) integration is required to compute the coefficients  $\Phi_{\mathcal{G}_i, \Sigma_j}$ ,  $\mathcal{G}_i(j)$  and  $\mathcal{G}_{i,i}^*$  of (18) so that an obvious significant reduction of the computational burden is expected. However, the computational effort to build the linear system (18) still scales as  $\mathcal{O}(n^2)$  as in classical BEM.

Lastly, note that the method can be applied to axisymmetrical problems where the fundamental solution is based on a complete elliptic integral of the first kind as it was shown by the author in [5].

### 2.2. FEM/FEM-Green Coupling

A complete set of equations associated with the hybrid FEM/FEM-Green is necessary to solve the whole problem. Then, the Galerkin problem related to the finite element domain  $\Omega_2$  has now to be derived. By referring again to Figure 1 and Equation (1b), the governing equation is either:

$$\nabla \frac{1}{\mu} \nabla A = 0 \quad \text{in } \Omega_2, \tag{22}$$

for general nonlinear magnetostatic problems, or

$$\nabla^2 A - j\omega\sigma\mu A = 0 \quad \text{in } \Omega_2, \tag{23}$$

in case of time-harmonic eddy-current problems.

The FEM problem is given by the respective Galerkin formulations

$$\int_{\Omega_2} \frac{1}{\mu} \nabla \hat{A} \cdot \nabla N_j \, d\Omega = 0 \quad \forall j \in \hat{\Omega}_2 \setminus \hat{\Gamma}_{int} \tag{24}$$

and

$$\int_{\hat{\Omega}_2} (\nabla \hat{A} \cdot \nabla N_j + j\omega\sigma\mu A) d\Omega = 0 \quad \forall j \in \hat{\Omega}_2 \setminus \hat{\Gamma}_{int}. \tag{25}$$

The Galerkin equation written for a node  $j$  belonging to the interface  $\hat{\Gamma}_{int}$  in a conventional FEM method would be:

$$\int_{\hat{\Omega}_1} \frac{1}{\mu_0} \nabla \hat{A} \cdot \nabla N_j d\Omega + \int_{\hat{\Omega}_2} \frac{1}{\mu} \nabla \hat{A} \cdot \nabla N_j d\Omega = \int_{\hat{\Omega}_s \subset \hat{\Omega}_1} J_s N_j d\Omega. \tag{26}$$

The right-hand side of (25) vanishes for nodes  $j$  that are not adjacent to the source region  $\hat{\Omega}_s$ . By introducing the expression (6) of  $\Phi_{\hat{A},\Sigma_j}$ , Equation (25) becomes:

$$\Phi_{\hat{A},\Sigma_j} + \int_{\hat{\Omega}_2} \frac{\mu_0}{\mu} \nabla \hat{A} \cdot \nabla N_j d\Omega = \int_{\hat{\Omega}_s \subset \hat{\Omega}_1} \mu_0 J_s N_j d\Omega \quad \forall j \in \hat{\Gamma}_{int}. \tag{27}$$

Finally, a global system of algebraic equations of the whole problem is obtained by an assembling procedure of Equations (18) and (24), or (25), and (27). It may be expressed as the partitioned matrix form:

$$\begin{pmatrix} -\mathbf{G}_{1i} & \mathbf{H}_{1i} & \mathbf{0} \\ -\mathbf{G}_{ii} & \mathbf{H}_{ii} & \mathbf{0} \\ \mathbf{1}_i & \mathbf{S}_{ii} & \mathbf{S}_{i2} \\ \mathbf{0} & \mathbf{S}_{2i} & \mathbf{S}_{22} \end{pmatrix} \cdot \begin{pmatrix} \hat{\Phi}_i \\ \hat{\mathbf{u}}_i \\ \hat{\mathbf{u}}_2 \end{pmatrix} = \mathbf{b}, \tag{28}$$

where the unknown vector  $\hat{\Phi}_i$  refers to the nodal flux values on  $\hat{\Gamma}_{int}$ , and vectors  $\hat{\mathbf{u}}_i$  and  $\hat{\mathbf{u}}_2$  are related to the nodal potential values on  $\hat{\Gamma}_{int}$  and  $\hat{\Omega}_2$ , respectively. Submatrices  $\mathbf{H}$  and  $\mathbf{G}$  represent the FEM-Green equations with the entries  $\Phi_{\mathcal{G}_{i,l},\Sigma_j}$  and  $\mathcal{G}_i(j)$ , or  $\mathcal{G}_{i,i}^*$ , respectively. The submatrix  $\mathbf{S}$  comes from the FEM contribution and  $\mathbf{1}_i$  is a unit matrix induced by (27). As it is the case for most FEM/BEM coupling methods, the global matrix has no particular structure, i.e., it is neither symmetric, nor positive definite. However, the  $\mathbf{G}$  submatrices are symmetric. A general solver must be used for the solution of the system (28), but the optimization of this specific point has not been investigated in the paper. Finally, vector  $\mathbf{b}$  relates to the source excitation  $J_s$  that appears in the right-hand side of (18) and (27).

### 3. Numerical Results

The method has been applied to two magnetic problems to estimate the performance of our numerical scheme. In the first example, a comparison with the classical FEM/BEM technique and the FEM with a large truncated outer boundary has been carried out to assess the accuracy of the method. As in previous papers of the author [4,5], all the algorithms were implemented in the MATLAB® environment on a standard desktop computer. The LU-decomposition was used for the solution of the involved linear systems. COMSOL Multiphysics® software has been used for the generation of the various meshes required by the simulations and also in order to confirm the results obtained by the FEM.

#### 3.1. Example 1—A Nonlinear Magnetostatic Problem

The first example is a 2D nonlinear magnetostatic problem defined on a C-shaped magnetic circuit  $\Omega_2$  with an excitation coil  $\Omega_s$  ( $J_s = 10^7$  A/m<sup>2</sup>) in air region  $\Omega_1$ , as depicted in Figure 4.

As an illustration, a magnetic field plot obtained by using COMSOL Multiphysics® is given in Figure 5. As classical FEM is used, the problem is encased in a circular box with a radius equal to about 15 times the mean size of the device. Magnetic induction along the line AB crossing the air gap, as shown in Figure 5, is plotted for the three methods in Figure 6. It is clear that FEM/BEM and FEM/FEM-Green methods are both in excellent agreement. Table 1 presents the magnetic energy restricted in an arbitrary rectangular domain of size  $0.6 \times 0.4$  m centered on the origin of the  $x - y$  reference frame

of the geometry and computed at a postprocessing step for both FEM/BEM and FEM/FEM-Green techniques. The number  $m$  of elements of magnetic and coil regions  $\Omega_2 \cup \Omega_s$ , is taken as a parameter. Convergence is observed and an extremely good agreement is obtained between the methods. A value of 74.53 J/m has been obtained with COMSOL in the same domain, by using a supplementary large external bounding rectangular box of size  $10 \times 10$  m. This result is in coherence with our results.

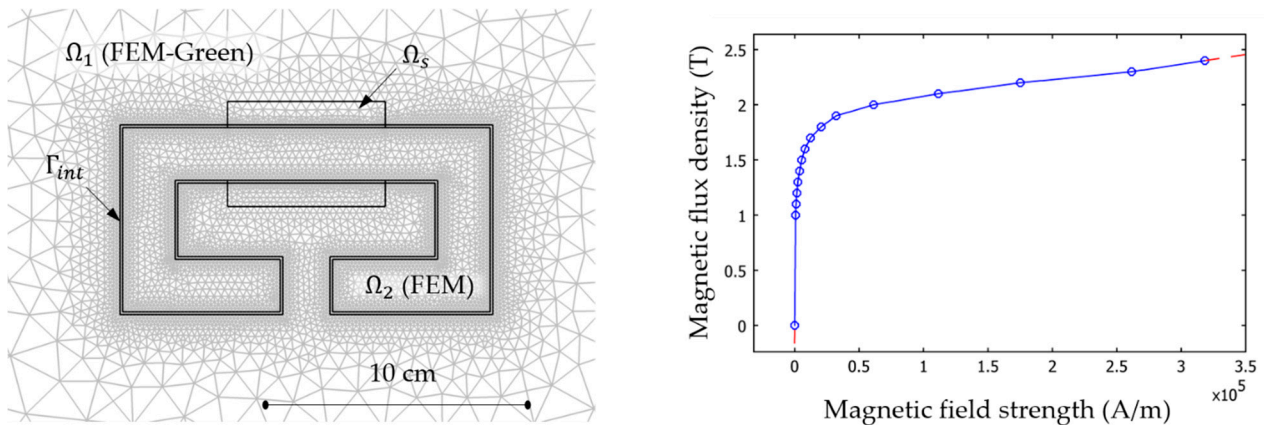


Figure 4. C-shaped magnetic circuit: mesh for FEM/FEM-Green treatment and B-H curve of the magnetic core material.

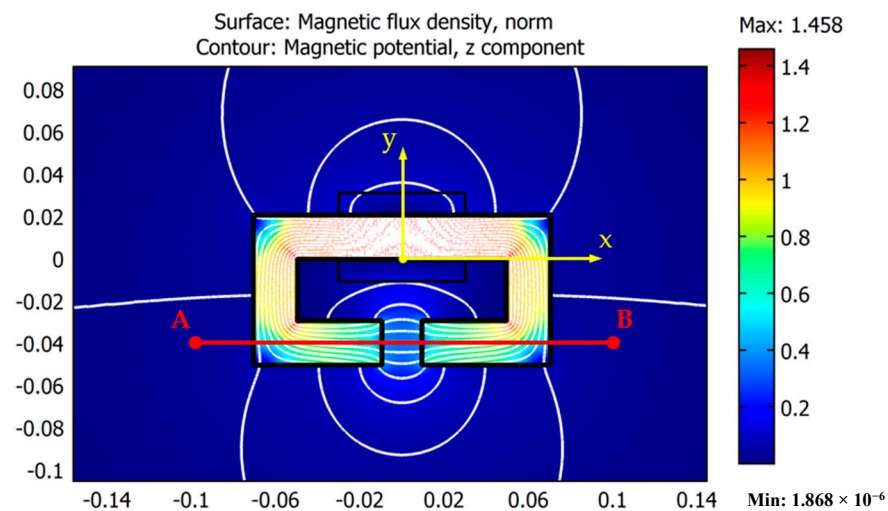


Figure 5. Plot of magnetic induction (in teslas) and field lines provided by COMSOL Multiphysics® package. Coordinate dimensions are in meters.

As already emphasized in [5], there is a lower computational burden in the FEM-Green part of the system (28), compared with the equivalent BEM part. However, global CPU times measured for both methods for the proposed example are not vastly different due to the important part involved in the solutions of the system at every iteration.

Table 1. Magnetic energy (J/m) in an embedding rectangular box vs. the number  $m$  of elements of the magnetic and coil regions.

$m$	FEM/BEM	FEM/FEM-Green
3204	76.33	75.35
4938	74.61	74.33
19,752	74.49	74.42
50,048	74.54	74.86



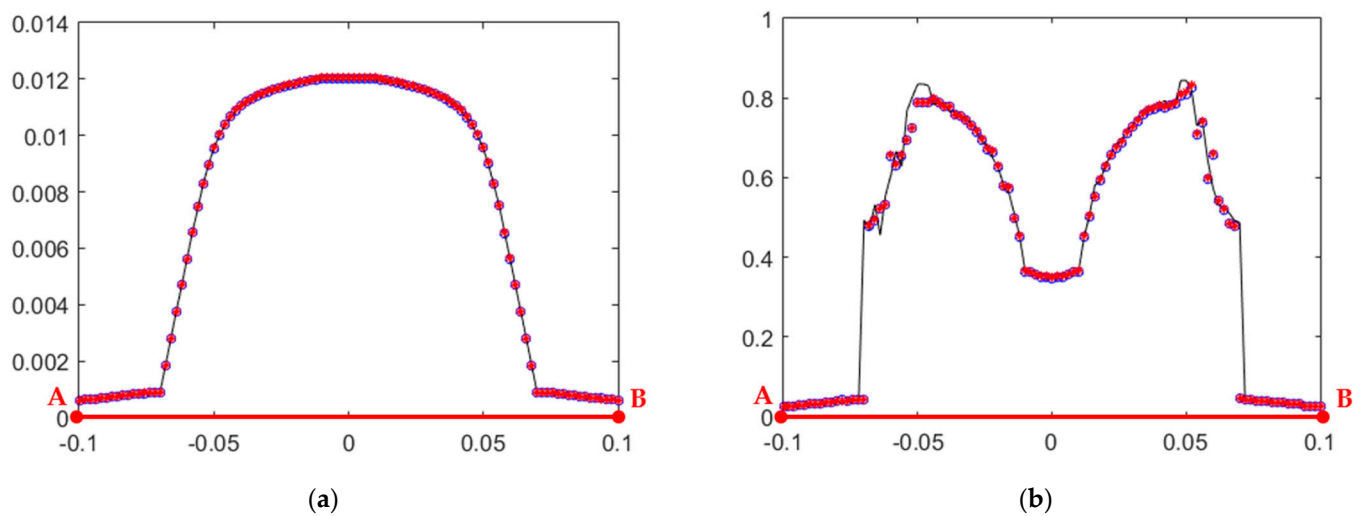


**Figure 6.** (a): Plot of magnetic vector potential (Wb/m) and (b) plot of magnetic induction (T) along the line AB for FEM (solid line), FEM/BEM (red stars) and FEM/FEM-Green (blue circles) methods. Abscissa in meters.

### 3.2. Example 2—Eddy-Currents in a Conducting Magnetic Region

The second example deals with a conducting region  $\Omega_2$  made of copper ( $\mu = 50 \times \mu_0$  H/m and  $\sigma = 5.998 \times 10^7$  S/m) and driven by source currents ( $J_s = 10^7$  A/m<sup>2</sup>, frequency = 5 Hz) located in region  $\Omega_s$ , embedded in air region  $\Omega_1$ , as presented in Figure 7.

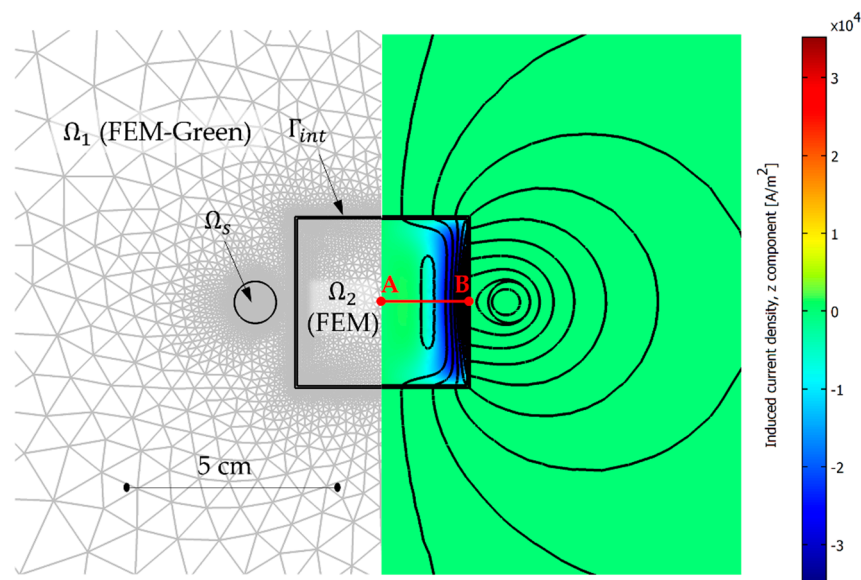


**Figure 7.** Eddy-current problem: mesh and results.

Time-harmonic modified Helmholtz equation is applied to this problem. COMSOL Multiphysics® solution is also given in Figure 7 where the induced current density is given by the statement:

$$J_i = -j\omega\sigma A. \tag{29}$$

Real and imaginary parts of  $J_i$  along the line AB crossing the conducting region is plotted in Figure 8 for FEM and FEM/FEM-Green methods (FEM-BEM is not applied here).

There is an excellent agreement between the results as the symbols  $\circ$  and  $*$  match the curves extremely well. The simulation has been realized with the number of triangular elements in conducting and source regions equal to 5811 as depicted in Figure 7.

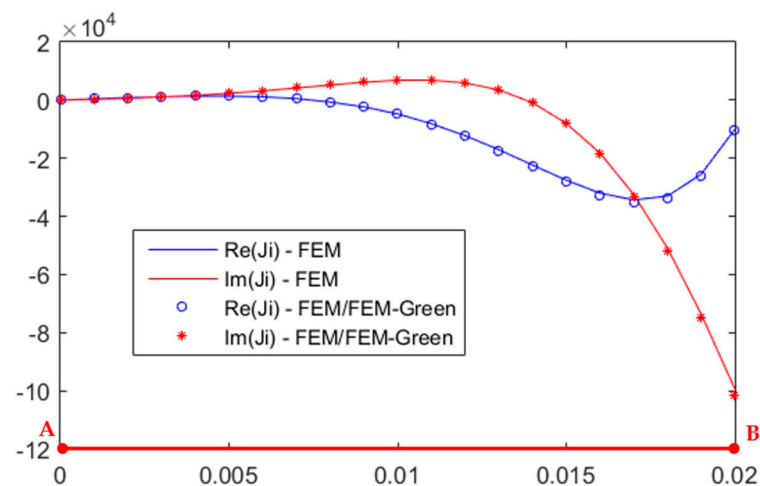


**Figure 8.** Plot of induced current density ( $A/m^2$ ) along line AB, obtained with FEM and FEM/FEM-Green methods. Abscissa in meters.

The losses have also been computed. A total of 9.45 mW/m has been obtained with the same mesh. This value should be compared with the value 9.42 mW/m computed with FEM and a circular box with a radius equal to about 100 times the mean size of the device. Those global quantities are quite similar considering the approximations that have been adopted.

### 3.3. Discussion

As a general comment about our method, some simulations have been carried out with a larger inside/outside interface around the active region, i.e., the magnetic circuit in the first example, eventually by including the excitation inside the FEM part. The same tests have been realized with the conducting part in the second example. The results are extremely close to each other in both cases.

However, we notice experimentally that it seems that a regular mesh with a single layer of triangle between the active (FEM) and outside parts gives a better accuracy of the method. Then, some precautions should be taken into account when preparing the mesh with our method. This is a constraint in our method that should be carefully considered at the programming stage.

## 4. Conclusions

The FEM/FEM-Green method presented in this paper has been proposed as an alternative to the classical FEM/BEM methods for the treatment of magnetic open boundary problems. The FEM-Green formulation applied to the open region is obtained by using the FEM approximation of fundamental solutions that leads to a discrete equivalent of the second Green's identity. The coupling with the finite element method used for the inner domains appears to be natural due to the same Galerkin approach in both mathematical treatments. Numerical results have pointed out an extremely good agreement between our technique and the standard hybrid FEM/BEM coupling that has been implemented for the sake of comparison. The advantages of the FEM-Green approach are an easier implementation since no particular integration is involved in the computation of the matrix coefficients, the absence of the somewhat awkward normal derivative of the fundamental solution in the formulation, and a more natural coupling with FEM. However, a layer of finite element mesh is required around the inner parts, and it should be carefully taken into account when programming the method. Our numerical scheme can be theoretically extended to 3D problems in the case of scalar potential applications (electrostatics, magnetostatics with scalar magnetic potential), and higher-order (e.g., quadratic) elements. In the latter case, there is no obvious geometrical interpretation of the nodal flux as with linear triangles, but it remains a representative variable. These aspects should be investigated in future work.

**Funding:** This research received no external funding.

**Institutional Review Board Statement:** Not applicable.

**Informed Consent Statement:** Not applicable.

**Data Availability Statement:** Not applicable.

**Conflicts of Interest:** The author declares no conflict of interest.

## References

1. Chen, Q.; Konrad, A. A Review of Finite Element Open Boundary Techniques for Static and Quasi-Static Electromagnetic Field Problems. *IEEE Trans. Magn.* **1988**, *24*, 80–85. [[CrossRef](#)]
2. Stephan, E.P. Coupling of Boundary Element Methods and Finite Element Methods. In *Encyclopedia of Computational Mechanics Fundamentals*, 2nd ed.; Stein, E., de Borst, R., Hughes, T.J.R., Eds.; John Wiley & Sons: Hoboken, NJ, USA, 2004; Volume 2, pp. 375–412. [[CrossRef](#)]
3. Brebbia, C.A.; Telles, J.F.C.; Wrobel, L.C. *Boundary Element Techniques, Theory and Applications in Engineering*; Springer: Berlin, Germany, 1984; pp. 400–426. [[CrossRef](#)]
4. Lobry, J. New boundary element formulation for the solution of Laplace's equation. In *Boundary Elements and Other Mesh Reduction Methods XLII*; Cheng, A.H.D., Tadeu, A., Eds.; WIT Trans. Eng. Sci.: Southampton, UK, 2019; Volume 126, pp. 63–73. [[CrossRef](#)]
5. Lobry, J. A New FEM–BEM Coupling for the 2-D Laplace Problem. *IEEE Trans. Magn.* **2021**, *24*, 80–85. [[CrossRef](#)]
6. Hartmann, F. *Green's Functions and Finite Elements*, 1st ed.; Springer: Berlin, Germany, 2013; pp. 109–208. [[CrossRef](#)]
7. Araya, R.; Behrens, E.; Rodriguez, R. A posteriori error estimates for elliptic problems with Dirac delta source terms. *Numerische Mathematik* **2006**, *105*, 193–216. [[CrossRef](#)]
8. Zienkiewicz, O.; Lyness, J.; Owen, D. Three-dimensional magnetic field determination using a scalar potential—A finite element solution. *IEEE Trans. Magn.* **1977**, *13*, 1649–1656. [[CrossRef](#)]
9. Chari, M.V.K.; Salon, S.J. *Numerical Methods in Electromagnetism*; Academic Press: San Diego, CA, USA, 1999; pp. 143–349. [[CrossRef](#)]
10. Bossavit, A. How Weak is the Weak Solution in Finite Element Methods? *IEEE Trans. Magn.* **1998**, *35*, 2429–2432. [[CrossRef](#)]